Electron plasma dynamics during autoresonant excitation of the diocotron mode

C. J. Baker,[a] J. R. Danielson,[b] N. C. Hurst,[c] and C. M. Surko[d]
Physics Department, University of California, San Diego, 9500 Gilman Drive, La Jolla, California 92093, USA

Chirped-frequency autoresonant excitation of the diocotron mode is used to move electron plasmas confined in a Penning-Malmberg trap across the magnetic field for advanced plasma and antimatter applications. Plasmas of 10^8 electrons, with radii small compared to that of the confining electrodes, can be moved from the magnetic axis to $\geq 90\%$ of the electrode radius with near unit efficiency and reliable angular positioning. Translations of $\geq 70\%$ of the wall radius are possible for a wider range of plasma parameters. Details of this process, including phase and displacement oscillations in the plasma response and plasma expansion, are discussed, as well as possible extensions of the technique. © 2015 AIP Publishing LLC. [http://dx.doi.org/10.1063/1.4907172]

I. INTRODUCTION

Single component plasmas (SCP) in Penning-Malmberg (PM) traps have proven useful for a range of fundamental physics studies as well as for applications.[1,2] In the PM trap, a uniform magnetic field provides radial confinement and electrostatic potentials on cylindrical electrodes at each end provide axial confinement. With care taken to avoid azimuthal asymmetries, SCP in PM traps exhibit excellent confinement properties to the extent that they can reach states in thermal equilibrium.[1]

A motivation of the research described here arises from the fact that SCP are the best known method to accumulate and store antimatter. This has led to the development of new techniques to accumulate and manipulate plasmas and tailor antiparticle beams for a range of antimatter studies. Examples include the development of high efficiency positron accumulators,[3] buffer gas and cyclotron cooling techniques,[2] and radial compression using rotating electric fields.[4,5] Beam techniques include advanced methods for spatial and time focusing, and the creation of beams with narrow energy spreads.[2] Numerous scientific accomplishments include studies of positron binding to matter,[6] the creation and trapping of antihydrogen,[7–9] and the formation and study of the dipositronium molecule.[10]

The desire to store larger numbers of antimatter particles (in particular positrons) for existing and planned research, particularly study of electron-positron many body physics,[11–13] provides strong motivation to develop higher capacity SCP traps.[2,14–16] One design for such a storage device[14,15,17] requires plasma to be moved large distances from the symmetry axis of a Penning-Malmberg trap. Another motivation for such a technique to move plasma across B is the development of an advanced technique for antihydrogen production.[18]

Described here is the exploration of a technique to translate plasmas across the magnetic field using chirped-frequency autoresonant excitation of the $l = 1$ plasma diocotron mode.[15,19] Plasmas can be moved efficiently and rapidly across the magnetic field in a PM trap and accurately positioned at a given radial and azimuthal location. The details of this process, current limitations, and potential improvements are discussed.

This paper is organized in the following way. Section II describes the apparatus and techniques used. Section III describes the plasma dynamics associated with the translation of a plasma to large displacements. Further studies of the details of plasma behavior are described in Sec. IV, followed by a set of concluding remarks.

II. OVERVIEW OF THE EXPERIMENTS

Details of the apparatus have been presented elsewhere.[17] The experiments are conducted in a multi-cell Penning-Malmberg trap, shown in Fig. 1, that consists of a master cell and four storage cells. All experiments were conducted in the master cell, which consists of five cylindrical electrodes of radius, $r_w = 38$ mm, for a total trap length $L = 304$ mm. One electrode (length 75 mm) is segmented azimuthally into four equal quadrants. This electrode structure is located within a $\sim 10^{-9}$ Torr vacuum system and immersed in a uniform axial magnetic field $B = 4.8$ T.

The parameters of the experiments described here are summarized in Table I. The data presented below primarily used two plasma lengths, a short plasma with plasma length $L = 40$ mm, and a long plasma with $L = 80$ mm. Plasmas are created in the master cell by scattering electrons from a beam into a potential well created by appropriately biased electrodes. The beam is generated from a heated cathode biased to -60 V. Plasma creation typically requires 8–12 s due to the relatively weak beam current (i.e., < 0.1 μA).

When required, sinusoidal voltages are applied to the segmented electrodes in order to compress the plasma radially to $r_p \sim 0.4$ mm and densities $n \sim 1 \times 10^{16}$ m^{-3} on a

[a]E-mail: cbaker@physics.ucsd.edu
[b]E-mail: jrdanielson@ucsd.edu
[c]E-mail: nhurst@physics.ucsd.edu
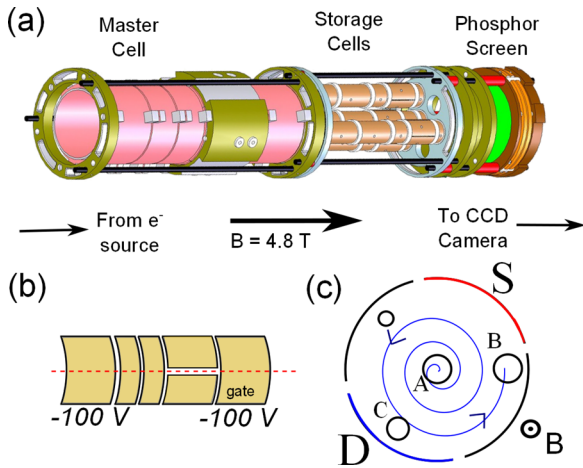[d]E-mail: csurko@ucsd.edu

FIG. 1. (a) Schematic diagram of the multicell-trap electrodes showing the master cell in which all experiments were conducted. Also shown are the four storage cells and phosphor screen for plasma imaging; (b) master cell schematic, with (- -) the symmetry axis; and (c) end view (as seen by the CCD camera) with (–) an outwardly spiraling autoresonant trajectory for an electron plasma. The storage cell electrodes, shown as circles (A–C), act as view ports. The drive (D) and received-signal (S) quadrants of the segmented electrode are labeled.

timescale $t_{RW} \sim 10$ s. Relays are used to switch in a damping circuit for ~200 ms to remove any remaining diocotron motion, followed by a cooling time of 1 s, where the 1/e cyclotron cooling time at 4.8 T is 170 ms.

For an infinitely long plasma at displacement d from the magnetic axis, the nonlinear diocotron frequency f_{NL} is

$$f_{NL} = f_1 \frac{1}{1 - (d/r_w)^2}, \tag{1}$$

where, in S. I. units,

$$f_1 = \frac{eN}{4\pi^2 \epsilon_0 L_p B r_w^2} \tag{2}$$

is the linear mode frequency, and it has been assumed that $r_p/r_w \ll 1$.

Equations (1) and (2) are only accurate for plasmas with $L_p/r_w \gg 1$, which is not true for plasmas in the master cell. However, numerical calculations including finite length corrections are in good agreement with measurements for the dependence of the mode frequency on d.[20,21] At very large

TABLE I. Typical plasma and autoresonance parameters, with B the magnetic field strength, r_w the wall radius, r_p the plasma radius, L_p its length, N the total electron number, n the plasma density, f_r the plasma rotation frequency, f_1 the linear diocotron frequency, V_0 the amplitude of the autoresonant drive signal, k the frequency chirp rate, and d/r_w the normalized plasma displacement.

Parameter	Value	Parameter	Value
B (T)	4.8	N	$(1-4) \times 10^8$
V_0 (V)	2–10	n (m^{-3})	$(0.04-1) \times 10^{16}$
k (kHz/s)	1–100	r_w (mm)	38
f_1 (kHz)	0.3 – 1	r_p (mm)	0.4 – 1
f_r (kHz)	120 – 450	L_p (mm)	40 – 120
d/r_w	0 – 0.95		

displacements (i.e., close to the electrodes), other effects, such as plasma shape changes, are important as well.[22,23]

Autoresonance is a generic nonlinear process by which an oscillatory mode of a system can phase-lock to an external drive. For this to occur, the oscillator frequency must be swept (i.e., chirped) through the linear frequency in the direction of increasing mode amplitude.[24] Once phase locking has occurred, the oscillator amplitude can be increased or decreased by changing the frequency of the drive.[19,24,25]

A simple model has been presented where the action of autoresonant locking occurs through the formation of a pseudopotential that traps the plasma.[19] In this pseudopotential, the plasma can exhibit small oscillations around the minimum, which will be observed as small phase and amplitude oscillations of the trapped oscillator. If the oscillations are too large, the oscillator will not be confined in the pseudopotential and the autoresonance will end. Thus, there is a minimum drive amplitude (i.e., depth of pseudopotential) for the oscillator to become locked to the drive.

In the case of autoresonant growth of the diocotron mode, the frequency increases with amplitude [cf. Eq. (1)], thus the chirp must start below, and extend to above f_1.[24] If the drive amplitude is sufficiently large, then the diocotron mode will increase in amplitude (d) with $f_{NL} \approx f_a$, where f_a is the applied frequency. During this process, the plasma executes an outwardly spiraling orbit such as that shown in Fig. 1(c).

To displace a plasma from the magnetic axis, an autoresonant drive signal is applied to a single quadrant of the azimuthally segmented electrodes of the form

$$V_D(t) = V_0 \sin [2\pi f_a(t)t], \tag{3}$$

where V_0 is the drive amplitude, and

$$f_a(t) = kt + f_0 \tag{4}$$

is the instantaneous frequency with k the chirp rate and f_0 the initial frequency, chosen here to be zero. Since this signal is applied to only one quadrant of the sectored electrodes, higher spatial harmonics could potentially become important at large d, but their effect was not studied systematically. Other functional forms for the "chirp" were briefly investigated (e.g., $f_a \propto k^t$). The result is that the late-stage, highest rate appears to dominate, and the results were similar to a comparable linear chirp.

To measure the plasma density profile and position, the gate electrode voltage (cf. Fig. 1(b)) is changed (typically from −100 V to ground) within ~2 μs, allowing the plasma to exit the trap. It is then accelerated to 5 kV and directed to a 94 mm diameter, P-43 coated, phosphor screen where the image is recorded using an Apogee A4000 CCD camera resulting in a spatial resolution ~55 μm.

III. PLASMA DISPLACEMENT STUDIES

Described here are studies to determine the maximum achievable plasma displacements in the plane perpendicular to B and the accuracy and reproducibility in radial and azimuthal position with which this can be done.

A. Induced-charge measurements

Plasmas in the master cell of the electrode structure shown in Fig. 1 could only be imaged at a restricted number of locations, which is accomplished by ejecting them through the four storage cells shown in Fig. 1(c). Thus, a complementary diagnostic of the plasma response to autoresonant drive was the image-charge signal picked up on a sectored ring, opposite that of the drive to minimize pickup, as illustrated in Fig. 2.

Shown in Fig. 3 is an example of autoresonant diocotron drive to final amplitude $d_f/r_w \sim 0.8$. In Fig. 3(a), the received signal vs. time is shown along with the applied (chirp) frequency. Figure 3(b), shows the experimental phase difference between the drive and measured diocotron mode (the π phase shift is due to the detector being on the opposite side from the drive). Finally, Fig. 3(c) shows, on an expanded scale, the drive and received signal during the last few cycles as the chirp ends and the plasma is ejected from the trap.

The entire autoresonant process is split into four regions. In region I, the drive frequency is below the linear frequency ($f_a < f_1$), thus there is no plasma response, and the phase varies continuously. In region II, the drive reaches f_1, and the diocotron mode becomes locked. This can be seen in Fig. 3(b) as the region in which the phase difference oscillates more slowly about π. As the frequency continues to grow, the mode amplitude also grows, accompanied by small amplitude and phase oscillations. The received mode signal is asymmetric in amplitude about 0 V due to the fact that the distance between the plasma and the segmented electrode varies over a cycle (cf. Fig. 2), and hence, so does the induced image charge.

The drive signal is terminated in region III (Fig. 3(c)), where the free-diocotron signal continues for several cycles. Termination of the drive signal typically is done when $V_a(t) = 0$ V (as in Fig. 3(c)), but termination at other phases does not appear to be deleterious. As discussed above, the free-diocotron and the final drive frequencies are typically not exactly the same, as a result of phase oscillations. Finally, in region IV, the plasma is ejected from the trap by lowering the gate potential.

The phase oscillations measured in Fig. 3(b) and the amplitude oscillations in Fig. 3(a) are directly related. The diocotron mode, although trapped in the pseudopotential well, can still have small oscillations about the well minimum, which depend on the amplitude of the drive.[19] Thus, during the time evolution, the mode frequency oscillates slightly around the trapped value, which leads to the varying phase difference during its trajectory. Further, since from
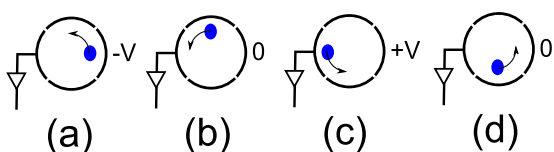

FIG. 2. Simplified schematic of plasma position (●) for four phases of the drive signal, (a) 0, (b) $\pi/2$, (c) π, and (d) $3\pi/2$ of the applied autoresonant drive. Note the image signal is received from the segment opposite the drive.
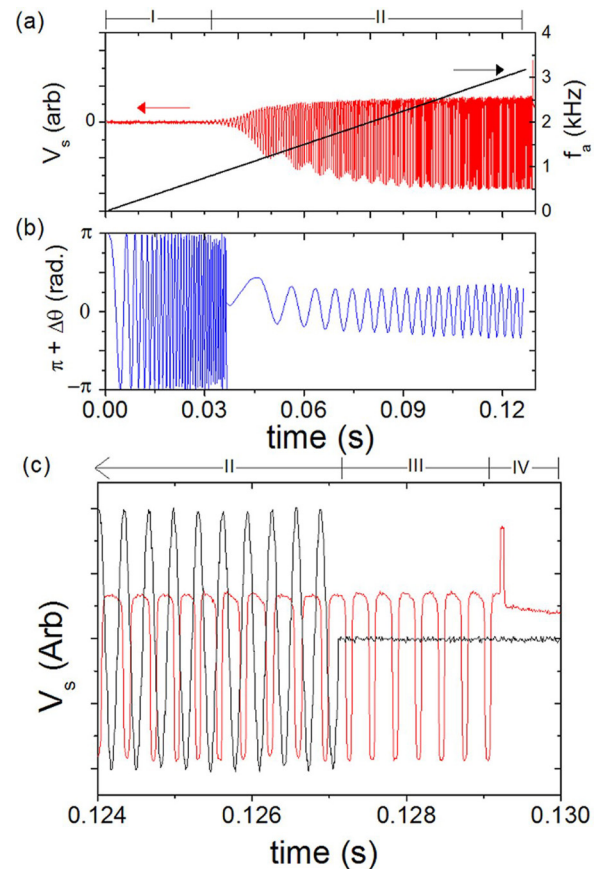

FIG. 3. (a) Pick-up signal (red line) with the autoresonant drive frequency (black line) shown for reference; (b) relative phase difference ϕ between drive and pick-up signals; and (c) the drive (black line) and pick-up (red line) signals during the last few cycles as the chirp ends. Data for the short plasma with $f_1^m \approx 1$ kHz, drive amplitude $V_0 = 2$ V, and chirp rate $\alpha = 25$ kHz/s. See text for details.

Eq. (1), the mode amplitude is directly related to its frequency, as the frequency oscillates, so does the mode amplitude. As shown below, if the drive amplitude is increased, these oscillations can be minimized.

B. Plasma displacements directly measured

Figure 4 shows the displacement d/r_w measured by ejecting the plasma through cell B (with center located at $d/r_w = 0.8$ and $\theta \sim 120°$ past the center of the drive electrode), and imaging it on the phosphor screen, as the final chirp frequency is varied at fixed chirp rate for two different drive amplitudes. The solid line in Fig. 4 is the prediction of Eq. (1) using the measured linear mode frequency, $f_1^m = 319$ Hz. The dashed curve, which is the prediction of numerical calculations including finite-length effects,[20,21,23] shows much better agreement with the measured frequencies.

As can be seen in the inset in Fig. 4, the 2 V drive case exhibits amplitude oscillations $\delta d/r_w \simeq \pm 0.02$. Note that for this plasma, $r_p/r_w \sim 0.03$, so these oscillations are on the same scale as the plasma size. In comparison, the 6 V drive case shows little oscillation. These data were taken at a fixed phase (i.e., $\theta \sim 120° \pm 2°$), not at a fixed time during the chirp. If there are phase/amplitude oscillations, the exact
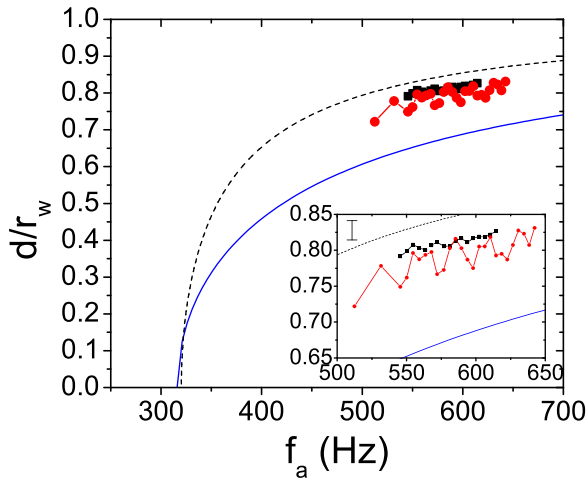
FIG. 4. Variations in radial displacement, measured by direct imaging, as a function of drive frequency during the autoresonant excitation. Displacements are measured $\sim 120°$ after the center of the drive electrode for 6 V (■) and 2 V (●) drive amplitudes. Lines joining the data are to guide the eye. The inset is an expanded range with the error bar indicating a typical plasma diameter. The solid line is Eq. (1) using the measured linear diocotron frequency, and the dashed line is from a numerical calculation including finite-length effects (see text for details).

time for a specific phase becomes difficult to predict. While these variations in phase and amplitude represent an important limit on the ability to position the plasma accurately, they can be minimized by operating at large drive amplitudes (e.g., the 6 V case in Fig. 4). In this case, the displacement accuracy is $\simeq \pm 0.3$ mm (i.e., $\simeq \pm 0.3 r_p$).

Fajans *et al.* predicted and experimentally verified the existence of a critical drive voltage, V_c, necessary for phase locking at a given chirp rate, k, where $V_c \propto k^{0.75}$.[19] If the plasma parameters change too rapidly or the pseudo potential well depth is too shallow, the mode does not remain phase-locked. Figure 5 shows the measured critical drive amplitude required for a plasma to be excited to a displacement in the range $0.65 \leq d/r_w < 0.8$ for various chirp rates. The fit to these data yields $V_c \propto k^{0.65 \pm 0.03}$, in reasonable agreement with the prediction of Ref. 19.

There are a number of effects that could contribute to the discrepancy between the $k^{0.65}$ scaling and the $k^{0.75}$ scaling reported in Ref. 19. For the long-plasma results presented
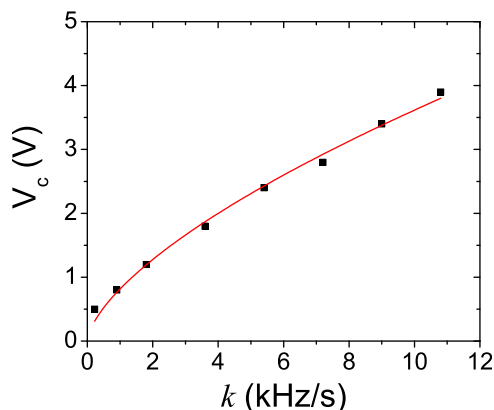
here, the transition between locked and unlocked is not sharp. When the diocotron mode was excited to $d/r_w \sim 0.5$, for example, the critical drive amplitude at a given chirp rate was lower than that shown in Fig. 5, although still consistent with a power-law dependence on k. In contrast, the critical drive in Ref. 19 was sharp (e.g., $\pm 2\%$). Other possible differences include the fact that the plasmas studied here exhibit a sharp increase in expansion at large displacements ($d/r_w > 0.7$); they sometimes extend into regions of nonuniform magnetic field; and they are confined in a low aspect ratio trap with $1 < L_p/r_w < 3$, leading to finite length effects (e.g., Fig. 4).

IV. PLASMA TRANSPORT DURING AUTORESONANCE

As discussed above, during autoresonant drive, the plasma is driven by an asymmetric voltage perturbation and can be moved to large off-axis positions close to the confining electrodes. This can have significant effects on the plasma, such as increased radial transport. By measuring plasma profiles for different experimental parameters, the processes of plasma expansion and charge loss were also investigated.

A. Directly measured plasma profiles

Figure 6 shows images of a plasma located near the trap axis (imaged through cell A), and three plasmas at large d: far from the drive electrode (B), near the drive electrode (C), and very near an electrode (B, elliptical image). The plasma profiles evolve from circular for all azimuthal locations at displacements $d/r_w \lesssim 0.8$, to elliptical at larger displacements. The ellipticity is greater when the plasma is near the drive electrode (e.g., C) and when larger drive amplitudes are used.
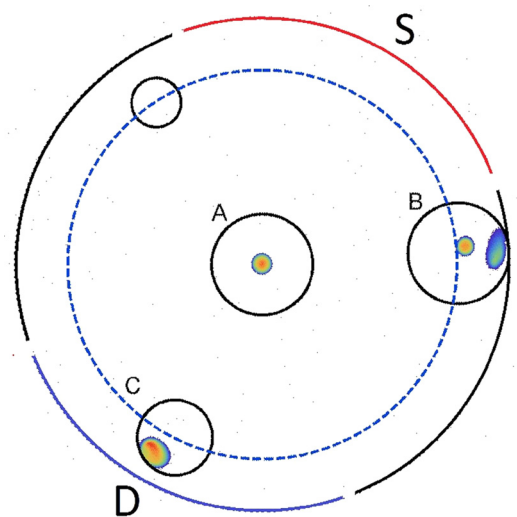

FIG. 6. Plasma density maps with trap viewing areas with (− −) $d/r_w = 0.8$ marked. Shown is a typical initial plasma viewed through window A; and through B, plasmas excited to $d/r_w = 0.82$ and $d/r_w = 0.95$. Note the extreme deformation and lower density of the outer plasma which is near the electrode. In the case of C ($\theta = 0°$), a plasma is excited to $d/r_w = 0.85$ and ejected rapidly; note the ellipticity due to the large drive amplitude. Drive and pick-up electrodes are labeled D and S, respectively.

FIG. 5. Critical drive voltage to excite a typical long plasma to $0.65 \leq d/R_w < 0.8$ for various chirp rates k. The fit (−) corresponds to $V_c \propto k^{0.65 \pm 0.03}$.

These observations are consistent with previous observations in that shape changes are observed when the plasma is close to a drive electrode,[26] or when d is so large that the plasma centroid is within a distance r_p of the wall.[22] While the plasma changes shape, $\langle r^2 \rangle$ remains the same.

B. Indirect plasma profile studies

Due to the limited possibilities for direct plasma imaging, a so-called "bidirectional" drive protocol, illustrated schematically in Fig. 7, was used to study profile changes over a greater range of d. The plasma was moved autoresonantly out to some displacement in time t_a (region I), then held there for time t_h at fixed frequency (region II), then the chirp was reversed, returning the plasma to the axis. Unfortunately, the reverse drive only moved the plasma to $d/r_w \sim 0.2$, due to loss of phase lock, and so feedback-damping was used to return the plasma to the axis rapidly (i.e., with little or no additional expansion). When t_a was kept the same for both processes, the plasma expansion during the chirp to large d was approximately the same as that during the reverse chirp.

C. Expansion and charge loss

Figure 8 shows data for the normalized rms final plasma radius $\tilde{r}$ as a function of the final displacement d_f, where

$$\tilde{r} \equiv \sqrt{\frac{\langle r^2 \rangle_f}{\langle r^2 \rangle_0}}, \tag{5}$$

with f and 0 denoting the final and initial states of the plasma. The data in Fig. 8 are taken using autoresonance at constant chirp rate $k = 2.5 \, \text{kHz/s}$ and varying the application time t_a. Data for two plasma lengths are shown: long ($L_p \sim 8 \, \text{cm}$) and short ($L_p \sim 4 \, \text{cm}$), as well as both small (2 V) and large (5–6 V) drive amplitudes. For these data, $t_h \ll t_a$, and so almost all the expansion occurs during the chirp.

For $d_f/r_w \leq 0.7$, there is little change in the plasma radius, while for $d_f/r_w > 0.7$, significant expansion is
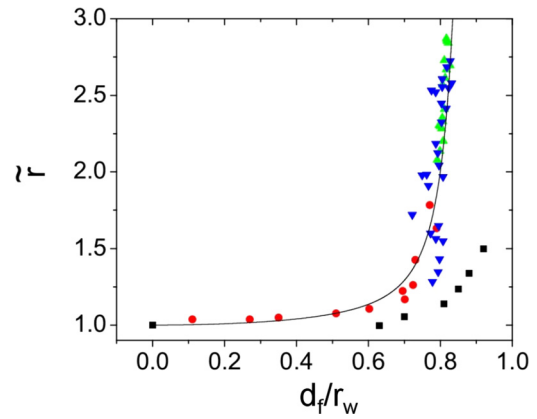

FIG. 8. Plasma radius (normalized to r_i) of long ($L_p \sim 8 \, \text{cm}$) and short plasma ($L_p \sim 4 \, \text{cm}$) containing $N \sim 1 - 4 \times 10^8 \, e^-$ as their final displacement, d_f, is varied (by varying t_a) at constant chirp rate, $k = 2.5 \, \text{kHz/s}$, with various drive amplitudes; short plasma with $V_0 = 2 \, \text{V}$ (■), long plasma with $V_0 = 2 \, \text{V}$ (▼), long plasma with $V_0 = 5 \, \text{V}$ (●), and long plasma with $V_0 = 6 \, \text{V}$ (▲). Data in the range $0.1 < d/r_w < 0.6$ were acquired indirectly using bidirectional drive, and the solid black line is a prediction from the model given in Eq. (6).

observed. This expansion is similar for the different drive amplitudes, although, as before, the low-amplitude drive exhibits significant amplitude oscillations. A key observation (discussed further below) is that the shorter plasmas exhibit less expansion and can achieve larger displacements, $d_f/r_w \geq 0.9$. Direct imaging of the plasma requires that the entire profile be visible through the storage cell. Thus, a short plasma with less expansion could be fully imaged for slightly lower d_f/r_w compared to a long plasma.

Charge loss is observed for long plasmas with aspect ratios $L_p/r_p \sim 200$ and initial radii 0.4–1 mm. Unfortunately, study of this effect is inhibited by the limited viewing opportunities. Fig. 9 shows the received image-charge signal for a plasma experiencing charge loss at $d/r_w \approx 0.8$ (while the autoresonant drive is still on). It shows charge loss over several diocotron periods, rather than as a single, catastrophic event. Similar plasma loss is observed for the short plasmas ($L_p/r_p \sim 30$), but only for small particle numbers $N < 1 \times 10^8 \, e^-$ and large drive amplitudes, $V_0 \sim 10 \, \text{V}$.
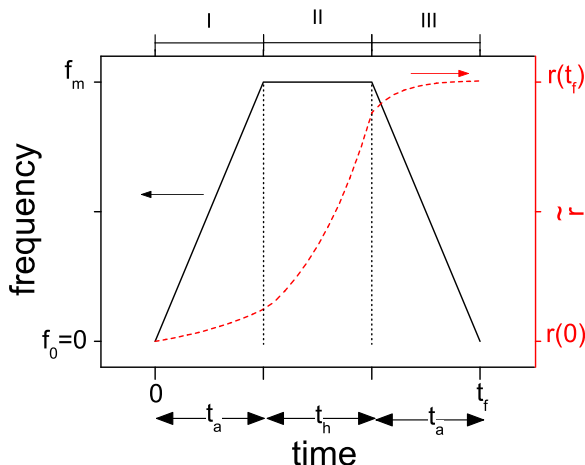

FIG. 7. Schematic diagram of the bidirectional autoresonance technique: (—) frequency, and (– –) plasma radius as a function of time, where t_a is the time duration of the frequency change to or from the maximum frequency f_m and t_h is the time f is held constant.
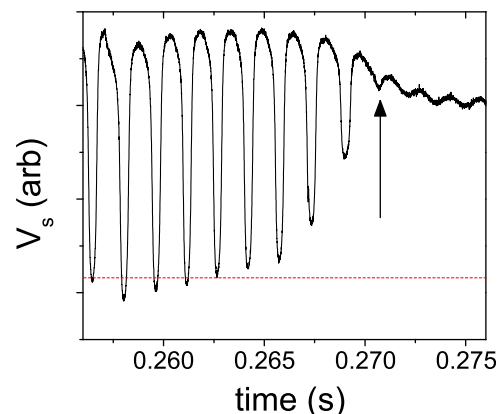

FIG. 9. Pick-up signal for a plasma excited to $d/r_w \approx 0.8$ while the drive amplitude is still on; (– –) indicates average peak amplitude for the preceding 70 ms (∼30 cycles), highlighting that the charge is lost in the final 2–3 cycles. Arrow indicates the point of total charge loss, which is followed by pick-up from the drive signal only.
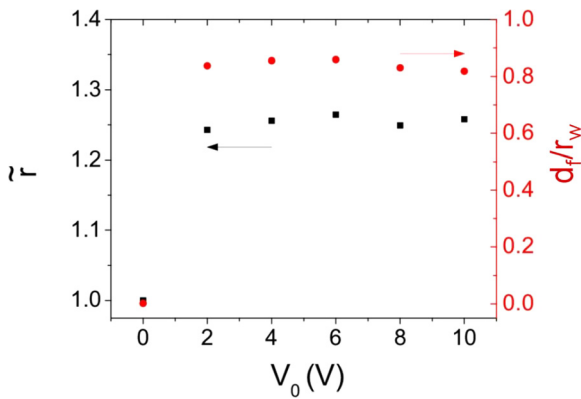
FIG. 10. (■) Variation of plasma radius (normalized to the initial radius) with drive amplitude V_0, applied for a fixed time t_a at constant chirp rate k; and (●) the corresponding displacement d_f/r_w.

Shown in Fig. 10 are data for the normalized, final plasma radius of a plasma excited to $d_f/r_w = 0.82$ for various drive amplitudes. The data show that the observed plasma expansion is independent of the drive amplitude, which is also consistent with the data shown in Fig. 8. Possible origins of this expansion include transport induced by mechanical imperfections and electrostatic "patch effects." The previously observed effect of "rotational pumping"[18,27] does not appear to be a significant contributor to the expansion on 100 ms timescales.

The possibility that the observed charge loss is due to a physical obstruction within the trap appears unlikely as the phase at which the plasma disappears is independent of the drive segment used. In a different experiment, charge loss by $\mathbf{E} \times \mathbf{B}$ flows along equipotential contours was observed when a large asymmetry is present.[21] However, as this has not been directly observed within the experiments presented here, we cannot confirm similar behavior.

Figure 11 shows the final radius of a short plasma with $L_p \sim 4$ cm excited to $d_f/r_w = 0.82$ in various times t_a, which is accomplished by varying the chirp rate (top scale). There appears to be a rapid expansion of $\sim 20\%$ for $t_a \leq 1$ ms, and then a cumulative effect based on the time the plasma spends at each displacement. The origin of the expansion at
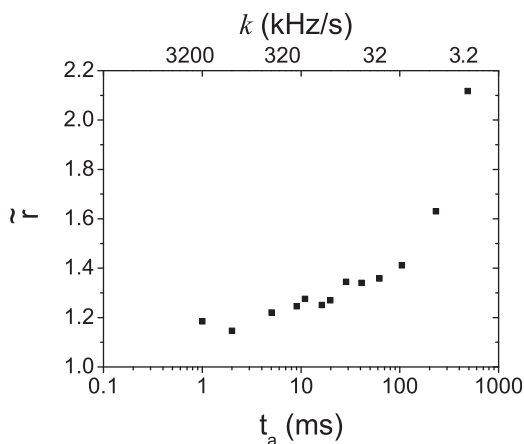

FIG. 11. Final plasma radius, at $d_f/r_w = 0.82$, normalized to the initial radius at $d = 0$, as a function of the autoresonant time t_a, on a semilogarithmic scale, for a plasma with $L_p \sim 4$ cm.
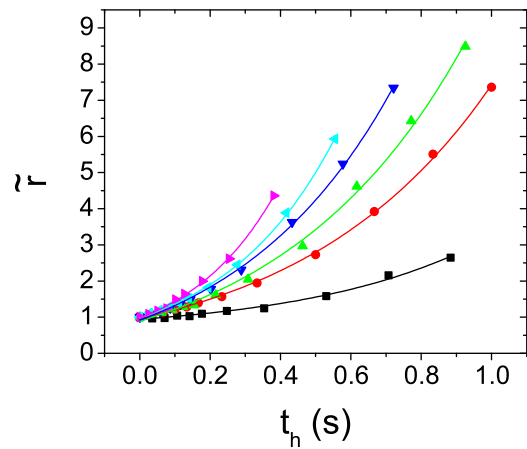

FIG. 12. Plasma radius, normalized to the radius for $t_h = 0$, as a function of hold time t_h at various displacements by varying t_a at constant chirp rate, $k = 2.5$ kHz/s: (■) $d/r_w = 0.43$, (●) $d/r_w = 0.52$, (▲) $d/r_w = 0.63$, (▼) $d/r_w = 0.67$, (◄) $d/r_w = 0.70$, and (►) $d/r_w = 0.76$. The data at each displacement (–) are fit with separate exponential functions to extract the expansion rate, $\Gamma(d)$.

$t_a \leq 1$ ms is presently unclear. The data in Fig. 11 indicate that it is possible to reach displacements $d/r_w \geq 0.8$ and accurately position the plasma in a few diocotron periods. For the fastest chirp rates, this can be done surprisingly quickly (i.e., in ~ 1.5 cycles of the drive signal).

In order to study the plasma expansion at fixed d, the bidirectional chirp was employed with various hold times t_h and final frequencies f_m for the two aspect ratio plasma. Figure 12 shows such data for a selection of displacements. While each plasma only permitted a small range of displacements to be investigated, overlap of data sets was possible at $d/r_w \sim 0.63$, and this enabled their normalization to remove the dependence on plasma length. Figure 13 presents the resulting expansion rates, $\Gamma \equiv d(\ln(\tilde{r}^2))/dt$, for various displacements. It indicates that the expansion rate increases very rapidly with d/r_w for $d/r_w \geq 0.6$. The solid curve in Fig. 13 is a fit to the data of the form, $\Gamma(x) = \Gamma_0(1 + \exp[(x - x_0)/\beta])$, with $\Gamma_0 = 1.6$, $\beta = 0.10$, and $x_0 = 0.7$, with $x = d/r_w$.

Using this fit for $\Gamma(d)$ and Eqs. (1) and (4), the expansion as a result of the plasma moving from $d = 0$ to some final displacement d_f can be calculated from
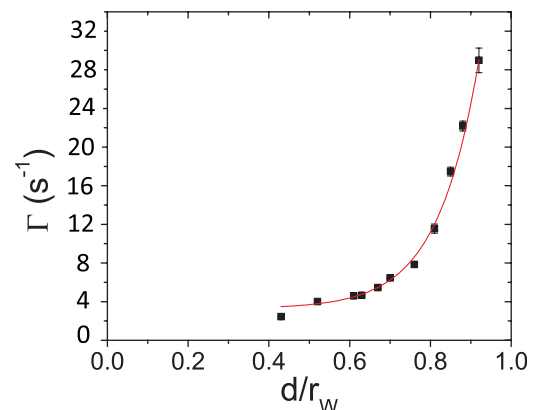

FIG. 13. Plasma expansion rate, calculated from the fits in Fig. 12, as a function of d/r_w. Also shown (–) is the fit to the data. See text for details.

$$\langle r^2 \rangle_f = \langle r^2 \rangle_0 \exp \left[\int_0^{d_f} (\dot{d})^{-1} \Gamma(d) \, \mathrm{d}d \right], \qquad (6)$$

where $\langle r^2 \rangle_f$ is the mean-square final radius, $\langle r^2 \rangle_0$ is the initial value, $\Gamma(d)$ is the plasma expansion rate at displacement d, and $\dot{d} = \mathrm{d}d/\mathrm{d}t$. Note that Eq. (6) depends on the chirp rate through the expression for $\dot{d}$.

The integral in Eq. (6) can be solved numerically. The results for the long plasma case are shown as the solid line in Fig. 8. The good agreement with the data indicates that the measured plasma expansion is independent of the autoresonance process and appears to be intrinsic to the Penning-Malmberg trap.

D. Dependence on location within the electrode structure

The plasma behavior described above appears to depend upon the axial location of the plasma in the electrode structure. The locations of plasmas investigated and the corresponding axial magnetic field profile are summarized in Fig. 14. Table II summarizes data for the plasma displacements achieved and the typical charge loss at that displacement for plasmas at these axial locations. A key result is that, for all plasmas studied, translation of the plasma to $d_f/r_w = 0.7$ could be achieved with little plasma expansion and no loss of particles (i.e., consistent with the data shown in Fig. 8). However, at larger displacements, there is sometimes charge loss (and enhanced expansion) for particular plasma locations and lengths.

In general, autoresonant positioning performance is better (larger displacements and less charge loss) for shorter plasmas in the region where there is less variation in B (cf. Fig. 14). In particular, plasmas corresponding to case A can be excited to the largest displacements with no charge loss, whereas performance degrades as the plasma occupies regions closer to the source. This appears to coincide with the region of $\sim$0.5% variation in the magnetic field, which can potentially cause particle trapping and plasma expansion.[28]
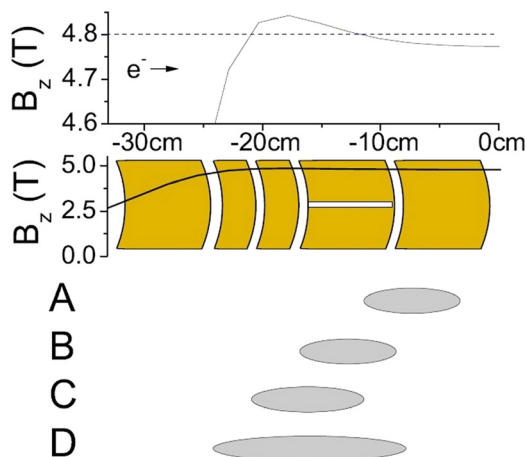

FIG. 14. (a) Expanded B_z field scale in trap region. (b) Schematic of trap electrodes with full range B_z field overlaid. (c) Plasma positions with respect to trap electrodes and B_z field.

TABLE II. Fraction of electrons remaining (N_f) after excitation to three different displacements d_f/r_w for the plasma locations indicated in Fig. 14.

Case	d_f/r_w	N_f (%)	d_f/r_w	N_f (%)	d_f/r_w	N_f (%)
A	0.9	100	0.86	100	0.7	100
B	0.92	90	0.81	90	0.7	100
C	0.89	46	0.85	74	0.7	100
D	N/A		0.79	100	0.7	100
			0.82	50	0.7	100

V. CONCLUDING REMARKS

Presented here is a study of the use of chirped-frequency autoresonant excitation of the $l = 1$ diocotron mode to translate plasmas in a Penning-Malmberg trap to large displacements from the magnetic axis and position them at precise locations in the plane perpendicular to B. Relatively short plasmas of 10^8 electrons with $L_p \sim 4$ cm and length-to-radius ratios $\sim$30 can be moved from the magnetic axis to $\geq$90% of the radius of the confining electrodes with unit efficiency. Furthermore, for all plasmas studied, displacements d/r_w up to 0.7 have been achieved with little change in the plasma parameters.

However, for long plasmas with $d/r_w > 0.7$, the plasma expansion is observed to increase rapidly with increasing displacement. Integrated over the plasma trajectory, this expansion results in a very sharp increase in the plasma radius near $d/r_w \sim 0.8$, resulting in particle loss, and limiting the maximum possible plasma displacement. While the origins of these effects are not currently understood, the inhomogeneous B field in the trap, used here for longer plasmas, is a possible contributor.

The fact that short plasmas can be translated rapidly to the largest displacements is an important result for the development of a multicell trap in that it also facilitates cell-to-cell transfer (e.g., see Ref. 17). In this regard, the use of large autoresonant drive amplitudes (i.e., $V_D \gg V_c$) facilitates improved positioning accuracy [e.g., $\pm$0.3 mm in radial, and $\pm$1 mm in azimuthal position at $d \approx 30$ mm ($\approx$0.8r_w)].

[1]D. H. E. Dubin and T. M. O'Neil, Rev. Mod. Phys. **71**, 87 (1999).
[2]C. M. Surko and R. G. Greaves, Phys. Plasmas **11**, 2333 (2004).
[3]T. J. Murphy and C. M. Surko, Phys. Rev. A **46**, 5696 (1992).
[4]F. Anderegg, E. M. Hollmann, and C. F. Driscoll, Phys. Rev. Lett. **81**, 4875 (1998).
[5]J. R. Danielson and C. M. Surko, Phys. Rev. Lett. **94**, 035001 (2005).
[6]G. F. Gribakin, J. A. Young, and C. M. Surko, Rev. Mod. Phys. **82**, 2557 (2010).
[7]M. Amoretti, C. Amsler, G. Bonomi, A. Bouchta, P. Bowe, C. Carraro, C. L. Cesar, M. Charlton, M. Collier, M. Doser, V. Filippini, K. S. Fine, A. Fontana, M. C. Fujiwara, R. Funakoshi, P. Genova, J. S. Hangst, R. S. Hayano, M. H. Holzscheiter, L. V. Jørgensen, V. Lagomarsino, R. Landua, D. Lindelöf, E. L. Rizzini, M. Macrì, N. Madsen, G. Manuzio, M. Marchesotti, P. Montagna, H. Pruys, C. Regenfus, P. Riedler, J. Rochet, A. Rotondi, G. Rouleau, G. Testera, A. Variola, T. L. Watson, and D. P. Van der Werf, Nature **419**, 456 (2002).

[8]G. Gabrielse, N. S. Bowden, P. Oxley, A. Speck, C. H. Storry, J. Tan, M. Wessels, D. Grzonka, W. Oelert, G. Schepers, T. Sefzick, J. Walz, H. Pittner, T. Hänsch, and E. A. Hessels, Phys. Rev. Lett. **89**, 233401 (2002).

[9]G. B. Andresen, M. D. Ashkezari, M. Baquero-Ruiz, W. Bertsche, P. D. Bowe, E. Butler, C. L. Cesar, M. Charlton, A. Deller, S. Eriksson, J. Fajans, T. Friesen, M. C. Fujiwara, D. R. Gill, A. Gutierrez, J. S. Hangst, W. N. Hardy, R. S. Hayano, M. E. Hayden, A. J. Humphries, R. Hydomako, S. Jonsell, S. L. Kemp, L. Kurchaninov, N. Madsen, S. Menary, P. Nolan, K. Olchanski, A. Olin, P. Pusa, C. Ø. Rasmussen, F. Robicheaux, E. Sarid, D. M. Silveira, C. So, J. Storey, R. I. Thompson, D. P. Van der Werf, J. S. Wurtele, and Y. Yamazaki, Nat. Phys. **7**, 558 (2011).

[10]D. B. Cassidy and A. P. Mills, Jr., Nature **449**, 195 (2007).

[11]P. M. Platzman and A. P. Mills, Phys. Rev. B **49**, 454 (1994).

[12]A. P. Mills, Jr., Nucl. Instrum. Methods B **192**, 107 (2002).

[13]T. S. Pedersen, J. R. Danielson, C. Hugenschmidt, C. Marx, X. Sarasola, F. Schauer, L. Schweikhard, C. M. Surko, and E. Winkler, New J. Phys. **14**, 035010 (2012).

[14]C. M. Surko and R. G. Greaves, Radiat. Chem. Phys. **68**, 419 (2003).

[15]J. R. Danielson, T. R. Weber, and C. M. Surko, Phys. Plasmas **13**, 123502 (2006).

[16]C. J. Baker, J. Jennings, A. Verma, J. Xu, M. H. Weber, and K. G. Lynn, Eur. Phys. J. D **66**, 109 (2012).

[17]N. C. Hurst, J. R. Danielson, C. J. Baker, and C. M. Surko, Phys. Rev. Lett. **113**, 025004 (2014).

[18]C. Canali, C. Carraro, D. Krasnicky, V. Lagomarsino, L. D. Noto, G. Testera, and S. Zavatarelli, Eur. Phys. J. D **65**, 499 (2011).

[19]J. Fajans, E. Gilson, and L. Friedland, Phys. Plasmas **6**, 4497 (1999).

[20]K. S. Fine and C. F. Driscoll, Phys. Plasmas **5**, 601 (1998).

[21]N. C. Hurst, J. R. Danielson, and C. M. Surko, "Finite length, high amplitude diocotron mode dynamics," AIP Conf. Proc. (unpublished).

[22]K. S. Fine, C. F. Driscoll, and J. H. Malmberg, Phys. Rev. Lett. **63**, 2232 (1989).

[23]R. L. Spencer and G. W. Mason, Phys. Fluids B **5**, 1738 (1993).

[24]J. Fajans, E. Gilson, and L. Friedland, Phys. Rev. Lett. **82**, 4444 (1999).

[25]J. Fajans and L. Friedland, Am. J. Phys. **69**, 1096 (2001).

[26]R. Chu, J. S. Wurtele, J. Notte, A. J. Peurrung, and J. Fajans, Phys. Fluids B **5**, 2378 (1993).

[27]B. P. Cluggish and C. F. Driscoll, Phys. Rev. Lett. **74**, 4213 (1995).

[28]D. L. Eggleston, K. J. McMurtry, A. A. Kabantsev, and C. F. Driscoll, Phys. Plasmas **13**, 032303 (2006).